ChemComm

FEATURE ARTICLE

View Article Online
View Journal | View Issue



Cite this: *Chem. Commun.*, 2019, 55, 2403

# Atomic layer deposition for efficient and stable perovskite solar cells

Seongrok Seo,[a] Seonghwa Jeong,[a] Hyoungmin Park,[a] Hyunjung Shin *[a] and Nam-Gyu Park *[b]

Organic–inorganic hybrid metal halides are now the most attractive photovoltaic absorber materials, typically, methylammonium lead triiodides ($MAPbI_3$). These unique semiconducting materials as absorbers demonstrate a remarkably improved power conversion efficiency of over 20% and now with a certified efficiency of 23.3%. Considering the Shockley–Queisser limit and their bandgaps, there is still much room to increase the efficiency. Stable devices with reproducibility and long-term use are essential for their commercialization. Atomic layer deposition (ALD) is a powerful technique to deposit high-quality thin films with excellent thickness accuracy and conformality, as well as with no pin-holes in a large area at low temperatures. ALD could be an ideal tool for efficient and stable perovskite solar cells. In particular, ALD will emerge for the production of tandem as well as flexible solar cells. This review contains the following recent research topics; underlying charge transport layers onto transparent conducting oxides (TCO), interfacial layers, overlying electron transport layers (ETLs), and encapsulation techniques utilized by ALD. Several extended understandings by recent studies and challenges toward further enhancing the efficiency and stability will be addressed.

Received 2nd December 2018,
Accepted 15th January 2019

DOI: 10.1039/c8cc09578g

rsc.li/chemcomm



## 1. Introduction

Organic–inorganic hybrid metal halides are now emerging as a new class of semiconductors. Known as the 'perovskite solar cell (PSC)', photovoltaic (PV) cells with $MAPbI_3$ (methyl ammonium lead triiodides), a notable example of a hybrid metal halide, as light-absorbing materials showed a remarkable power conversion efficiency (PCE) of over 20%.[1–11] The certified PCE is currently 23.3%.[12] PSCs have attracted considerable attention due to their rapid increase in absolute efficiency per year (%) of 2.27 from that of the first solid-state PSCs of 9.7%[3] up to the currently highest certified PSC within recent six years, which has largely surpassed other types of solar cells, increasing by under 1.0% per year.[12] The PCE enhancements were achieved through scientific understanding as well as by engineering advancement. The former includes crystal growth, compositional modification and optoelectronic properties of the perovskite film, and the latter signifies interfacial modification and the development of highly efficient charge transport layers (CTLs) in the cells.[13–16]

PSCs have a sandwich structure of the perovskite layer, which absorbs sunlight and generates photo-excited carriers, and CTLs, which transport the photo-excited carriers to the electrodes. In addition, CTLs are divided into electron transport layers (ETLs), which transport photo-excited electrons, and hole transport layers (HTLs), which transport holes. The typical structures of PSCs can be represented by three different types as shown in Fig. 1, which are mesoscopic n–i–p, planar n–i–p and p–i–n structures, respectively, and the types of PSCs are named according to the CTLs in which the sunlight passes through first. In the mesoscopic structure, a bilayer using a compact layer and a nanostructured/mesoporous material is used as an ETL, whereas in a planar structure, only a compact layer is used as CTLs. Since the ETL extracts and transport electrons, n-type materials were used, and the conduction band (CB) minimum should be positioned lower than that of the perovskite. On the other hand, the HTL requires p-type materials, and the valence band (VB) maximum must be shallower than that of the perovskite. Most typical n–i–p PSCs include $TiO_2$ as ETL and 2,2′,7,7′-tetrakis(*N*,*N*-bis(*p*-methoxyphenyl)amino)-9,9′-spirobifluorene (Spiro-OMeTAD) as the HTL, and the p–i–n includes poly(3,4-ethylenedioxythiophene):poly(styrene-sulfonate) (PEDOT:PSS), poly[bis(4-phenyl)(2,4,6-trimethylphenyl)amine] (PTAA) and 1-(3-methoxycarbonyl)propyl-1-phenyl-[6,6]$C_{61}$ (PCBM). Inorganic materials have been intensively studied as CTLs to enhance the stability of PSCs. Representative inorganic materials of ETLs include $TiO_2$,[14] $SnO_2$,[17] ZnO,[18] $Zn_2SnO_4$[19] and $BaSnO_3$,[20] and those of HTLs include NiO,[21] $CuO_x$,[22] CuI,[23] $CrO_x$,[24] Cu-based delafossite materials[25–27] and high-work-function $MoO_3$.[28] Among the many candidates, ETLs such as $TiO_2$, $SnO_2$, ZnO and NiO HTL layers can be deposited

[a] *Department of Energy Science, Sungkyunkwan University, Suwon 440-746, Republic of Korea. E-mail: hshin@skku.edu*
[b] *School of Chemical Engineering, Sungkyunkwan University, Suwon 440-746, Republic of Korea. E-mail: npark@skku.edu*

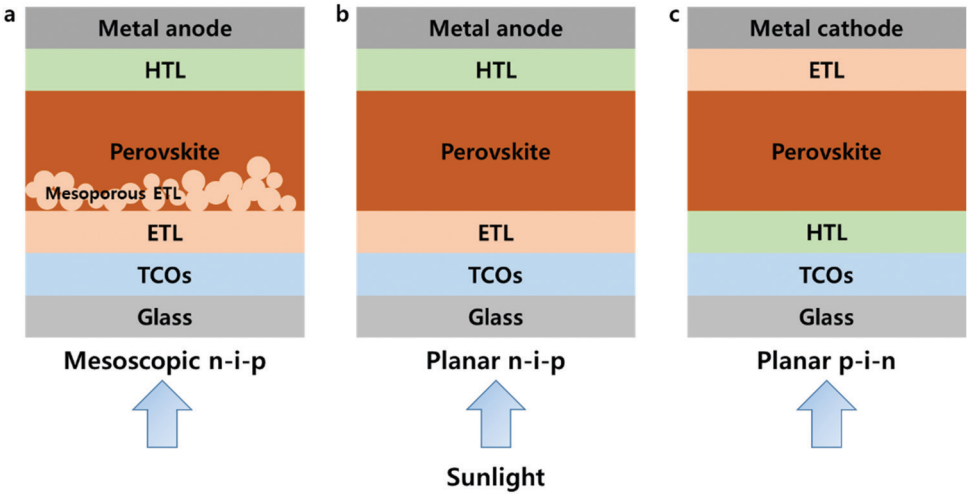


Fig. 1 Typical three structures of the PSCs. The bilayer of compact and mesoporous materials consists of the ETL in mesoscopic n–i–p structure (a), and only compact ETL and HTL are used in planar n–i–p structure (b) and p–i–n structure (c).

through atomic layer deposition (ALD) processes; in addition, $Al_2O_3$ which does not act as a CTL due to its insulating property but is used as a passivation layer, is also capable of ALD processes.[29,30]

ALD is a powerful tool to deposit films on the substrates, with a high conformality that can be hardly achieved by any other technique. Dr Tuomo Suntola first invented atomic layer epitaxy (ALE, commonly used term prior to 2000, instead of ALD) in the 1970s.[31] In his paper, the development of electroluminescent flat panel displays using ZnS thin films grown *via* ALE was reported.[2] During the past decades after the invention, enormous materials as well as growth methods *via* ALD have been developed.[32] The application of ALD has been largely devoted to the microelectronic industry and nanotechnology.[32] In recent, many studies have focused on the application of ALD to renewable energy devices including photovoltaics (PVs).[33,34]

ALD is comprised of a binary sequence of self-limiting chemical reactions between gas-phase precursor molecules and a solid surface, which is solely dependent on the properties of the surface. This self-limiting nature of the ALD gives rise to conformal growth behavior and additional control over the total thickness of the film. The precise film thickness control can be realized simply by the repeating number of coating cycles. The schematic typical ALD process is described in Fig. 2. A cycle of the ALD process consists of four steps: the A source pulse, purging and the B source pulse, and purging. Injecting the A source into the reaction chamber together with the carrier gas (usu. $N_2$, Ar, *etc.*) causes the A molecule ($Zn(CH_2CH_2)_2$ (diethylzinc, DEZ), $Al(CH_3)_3$ (trimethylaluminium, TMA), *etc.*) to be chemisorbed on the substrate, and then injecting the B ($H_2O$, $H_2O_2$, $H_2S$, *etc.*) source into the substrate induces a self-limiting reaction between the chemisorbed A and B sources. The remaining surplus B sources will be removed through purging. The self-limiting reaction refers to the reaction of the reactant sources A and B only on the surfaces, not the reaction between sources off of the surface. We briefly introduce the surface chemistry of $Al_2O_3$ using TMA and $H_2O$ in ALD, which was well-established as a model system:[35]

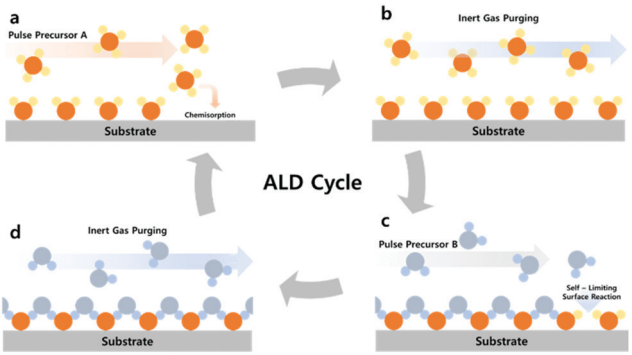


Fig. 2 Schematic representation of the typical ALD process; (a and c) A and B source precursor pulse; (b and d) inert gas purging of the remaining (unreacted) precursor source.

$$\text{(A)}\ -\text{AlOH}^* + \text{Al(CH}_3)_3 \rightarrow \text{AlOAl(CH}_3)_2^* + \text{CH}_4(\text{g}) \quad (1)$$

$$\text{(B)}\ -\text{AlCH}_3^* + \text{H}_2\text{O} \rightarrow \text{AlOH}^* + \text{CH}_4(\text{g}) \quad (2)$$

$$\text{(C)}\ 2\text{Al(CH}_3)_3 + 3\text{H}_2\text{O} \rightarrow \text{Al}_2\text{O}_3 + 3\text{CH}_4(\text{g}) \quad \Delta H = -376\ \text{kcal} \quad (3)$$

where the asterisks represent the surface species. The overall reactions are self-limiting and spontaneous, which leads to the formation of a strong Al–O bond. The reaction of the alternating exposure of sources was repeated to produce the desired thickness of the $Al_2O_3$ films by increasing the number of cycles.

Taking advantages of the self-limiting chemical surface reactions, ALD can guarantee high uniformity in a large area, conformality and a nm scale thickness control of films. Furthermore, ultra-high aspect ratio (more than 500 : 1) substrate structures can be conformally deposited by ALD.[36,37] Unlike conventional CVD that attaches a compound to a substrate, ALD has the advantage of deposition at relatively low temperatures ($<200\ ^\circ$C) because it atomically grows the compound on the substrate, which is applicable to any flexible devices. Typical binary compounds

 

that can be deposited with ALD include many different metal oxides, sulfides, and nitrides, for example, $TiO_2$, $ZrO_2$,[38] $Al_2O_3$,[39] NiO,[40] $SnO_2$, $MoS_2$,[41] and TiN.[42] The greatest advantage of applying ALD at the fabricating CTLs is the possibility of depositing thin films without any pinholes and/or electrical leakages. As a result, conformal and pinhole-free CTLs by ALD can be considered as important components in PSCs in improving efficiency as well as stability.

The substantial importance of the ALD process for PSCs has since been reported; an overview of the ALD application for PSCs will extend the understanding of the engineering of PSCs. There are two review papers concerning ALD for PSCs thus far. Deng and Li reviewed several selected articles to emphasize the importance of the ALD process for the engineering of PSCs.[29] In another perspective article, Zardetto *et al.* offered a considerably complete review of several ALD-grown materials utilized for PSCs. Some important aspects of the ALD process for PSCs by the two reviews were well presented.[30] They have not sufficiently covered the newly discovered importance of overlying ETLs onto the perovskite for stability improvement and practical cases of encapsulation engineering, which is recently progressed. In this review, we focused on ALD processes for highly efficient and stable PSCs including underlying charge transport layers onto transparent conducting oxides (TCO), interfacial layers, and overlying ETLs, and encapsulation techniques using ALD. To conclude, several extended understandings by recent works and challenges toward further enhancing efficiency and stability will be addressed.

## 2. ALD for PSCs

### 2.1 Underlying charge transport layers (CTLs)

CTLs play an important role in the performance of PSCs, which selectively extracts photo-generated charges from the perovskite layer and transport them to the electrodes. Underlying CTLs, which are processed onto TCOs such as fluorine-doped tin oxide (FTO) and indium tin oxide (ITO), largely affect the growth of the perovskite layer due to the interaction between substrate CTLs and perovskite precursor solutions. Underlying CTLs require the following characteristics, regardless of the ETL or HTL: (1) charge selectivity, having a slightly lower conduction band as the ETL and/or higher valence band alignment as the HTL relative to that of the perovskite; (2) high conductivity, with high charge carrier mobility for efficient charge extraction and transport; (3) film morphology, granting pinhole-free dense morphology reducing current leakages through shunt pathways; (4) chemical stability, to avoid chemical reactions between the underlying CTLs and the perovskite; (5) transparency, affecting the amount of light reaching the perovskite layer mostly with wide-band gap CTLs.

The reduction of CTL thickness can reduce the serial resistance of the device due to the short transfer distances of the photo-generated charges. Processing such a thin film, however, has been challenging in most cases, since thin film processing usually resulted in pinholes and cracks, leading to a reduced charge carrier blocking probability and creating a shunt leakage pathway. Furthermore, in the case of large area substrates and/or substrates with a high-aspect ratio, the formation of ultra-thin films with uniform thicknesses is even more challenging. ALD can provide ideal CTLs with conformal and dense film growth followed by precise sub-nanometer scale thickness control. Roselofs *et al.* recently introduced the impact of conformality for ultrathin 4 nm compact $TiO_2$ layers for mesostructured PSCs.[43] They found that the high conformality by ALD allows the use of 4 nm thick $TiO_2$ instead of ~50 nm thick $TiO_2$ by spray-pyrolysis as shown in Fig. 3a and b. The devices fabricated from both $TiO_2$ films showed similar PCEs of around 11.5%. Although the impact of conformality by ALD has been demonstrated, 4 nm $TiO_2$ was formed with the rutile phase. As such, the conduction band lies 0.2 eV below that of the anatase.[44] The benefit of ultrathin $TiO_2$ in this study remained unclear. Seo *et al.* proposed the thickness effect of ultrathin NiO as a HTL as shown in Fig. 3c.[40] Where the film thickness is sufficiently thin to be affected by the characteristic length of the space charge region, Debye length ($L_d$),

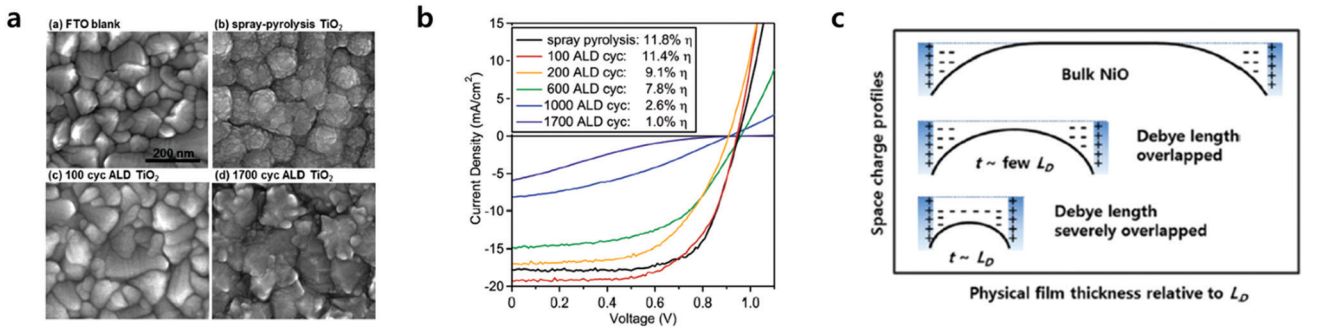


Fig. 3 (a) SEM images of $TiO_2$ films grown on FTO, all at the same magnification with a 200 nm scale bar. (b) Performance of representative mesoporous perovskite solar cells with 50 nm thick spray-pyrolysis compact $TiO_2$ layers, compared to varied thicknesses of ALD $TiO_2$ from 100 ALD cycles (4 nm thick) to 1700 ALD cycles (90 nm thick). Plotted are the settled *J*–*V* performance under 1 sun of AM 1.5 illumination. Reproduced with permission.[43] Copyright 2016, Wiley-VCH. (c) Schematic images of physical films' thickness relative to the Debye length ($L_D$) *vs.* space charge profiles. When the thickness of NiO films is large enough compared to the $L_D$, the NiO films were bulk-like, thus insulating ones as shown in the inset (top). Once the films' thicknesses were thin enough, the $L_D$ started to overlap, and thus the apparent work function and hole concentration are increased (schematic in middle). Even in thinner films, $L_D$ is severely overlapped (schematic in the bottom). Reproduced with permission.[40] Copyright 2016, The Royal Society of Chemistry.

the films can exhibit higher electrical conductivity relative to that of the bulk film. They found an apparent increase of the electronic concentration of NiO films below ~7 nm, which addressed the beneficial effect of ultra-thin transport layers on the device performance. Taking advantage of the precise thickness control in conformal ALD, ALD-grown CTLs with a thickness of a few nanometers have been used for efficient PSCs. The most widely investigated ETLs and HTLs grown *via* ALD as the underlying layers are summarized in Table 1.

The initial ALD ETL study on underlying ETLs based on $TiO_2$ focused on the clarification of the superiority of the ALD process compared to other solution-processes, *i.e.*, mostly sol–gel spin coating and spray-pyrolysis.[43,45–48] Lu *et al.* fabricated pinhole-free and compact ETL $TiO_2$ films processed by ALD for planar n–i–p PSCs as shown in Fig. 4a.[49] ALD $TiO_2$ showed a better PCE of 13.6% compared to that of solution-processed $TiO_2$ (*i.e.*, 8.7%). They have figured out that the optimum thickness of ALD $TiO_2$ is 10 nm where PSCs exhibit the best performance. PSCs with ultra-thin ALD $TiO_2$ films (5–20 nm) showed better photocurrent compared to those with solution-based $TiO_2$, thanks to the excellent transmittance in the wavelength range of 400–900 nm. They also found that the ALD $TiO_2$/perovskite interface generates less leakage current, due to the dense and pinhole-free film quality provided by ALD.

Lu *et al.* have subsequently proposed that the conduction band edge and Fermi level of ALD $TiO_2$ has been slightly shifted shallower relative to that of solution-processed $TiO_2$ due to the higher concentrations of $Ti^{3+}$ defects and surface absorbed –OH groups in the film, evidenced by X-ray photoelectron spectroscopy (XPS).[47] Utilizing these energy level differences, they formed a solution-based $TiO_2$/ALD $TiO_2$ bilayer ETL with type II band alignment and recorded a PCE of up to 16.5%. In spite of demonstrations of the superiority of the ALD process, it hardly obtained highly efficient planar PSCs based on $TiO_2$, noted by the poor interface between the $TiO_2$/perovskite regardless of the processes.[50] It has been proposed that interfacial modification,[13] or the doping[51] strategy of solution-processed $TiO_2$ could improve the performance of planar PSCs. Zardetto *et al.* reported that the interfacial property between the ALD $TiO_2$/perovskite can be improved by the surface treatment of $CF_4$ gas under plasma.[52] $CF_4$-treated $TiO_2$ has a deeper energy level compared to the pristine one, which allows better formation of the band alignment with the perovskite layer and facilitates electron extraction. In addition, the surface of $CF_4$-treated $TiO_2$ improved the interfacial adhesion when perovskite-coated, increasing the maximum PCE up to 14.8% from 4% (Fig. 4b).

The application of ALD $SnO_2$ layers in planar PSCs was more successful than ALD $TiO_2$ ones in terms of their PV performances. Correa *et al.* firstly reported that the planar PSC based on ALD $SnO_2$, deposited at a low temperature of 118 °C, recorded a maximum PCE of 18.4%.[53] They observed that ALD $SnO_2$ forms barrier-free band alignment with mixed cations halides perovskite layers ($(FAPbI_3)_{0.85}(MAPbBr_3)_{0.15}$). Furthermore, an efficient extraction of the electrons from the perovskite into $SnO_2$ was proven by femtosecond transient absorption (TA) measurement. Consequently, PSCs with ALD $SnO_2$ show no current–voltage hysteresis or reproducible current–voltage characteristics regardless of scan rates (Fig. 5a). The importance of band alignment between ETL/perovskite in planar PSCs was well highlighted. In their later study, $SnO_2$ was passivated by thin (<1 nm) $Ga_2O_3$ interlayers for the sake of the suppression of interfacial recombination.[54] However, the passivation of $Ga_2O_3$ did not show any improvement in PV performances. In addition, they have confirmed that interfacial recombination near $SnO_2$ is considerably well suppressed by the intrinsic interfaces between the ALD $SnO_2$/perovskite layers. Based on this ALD layer, which is energetically favourable with the perovskite, they reported that the incorporation of RbI into the MAFA-based perovskite can enhance the lifetime of charge carriers up to 1.37 μs (0.55 μs for non RbI-perovskites) and promote hysteresis-less current–voltage characteristics, eventually yielding a PCE of 20.3% (Fig. 5c).[13] Furthermore, It was demonstrated that the $V_{oc}$ of the device could be enhanced to 1.23 V (just 100 mV lower than the thermodynamic limit) through the control of the doping level of HTL (Spiro-OMeTAD).[14]

It is well known that the material properties of a semiconductor can typically be improved through high-temperature-induced recrystallization. In contrast, Lee *et al.* reported high-temperature (300 °C) annealed $SnO_2$ layers largely decreased the performance of PSCs, while annealed $SnO_2$ ones at mild temperatures (180 °C) showed better PV performances (Fig. 6).[55] This trend has been consistently observed in PSCs not only with ALD $SnO_2$ layers but also in other solution-processed $SnO_2$ layers.[56,57] They suggest that residual precursors, tetrakis(dimethylamino)tin (TDMASn) in case of the ALD process, in the $SnO_2$ films decompose at high temperatures of 230 °C, leaving highly conductive $SnO_2$ layers. The contrasting behavior of annealed $SnO_2$ layers is ascribed to the reduction of the hole-blocking ability due to metal-like nature of $SnO_2$. As a result, they were addressed as-deposited and mildly annealed $SnO_2$ films containing self-passivating residual precursors, which is inevitably required to provide good electron mobility as well as hole-blocking property.

Several $SnO_2$ *via* plasma-assisted ALD applied to planar PSCs has also been investigated.[58–61] Wang *et al.* further reduced the process temperature of $SnO_2$ to 70 °C thanks to the additional energy from plasma, which resulted in the maximum PCE of 19%.[60] They utilized $C_{60}$-SAM as an interfacial modifier on $SnO_2$ to suppress the interfacial recombination. Considering its high electron mobility as well as its energy level position, $SnO_2$ is one of the most suitable candidates in planar PSCs. Many researchers have considered doping strategies to obtain better electron transfer within $SnO_2$ due to its wide band gap nature.[62] However, it is not the desired process because the doping process also frequently requires high-temperature annealing. Thus, $SnO_2$ *via* the ALD process, capable of sub-nanometer thickness control of the thin film, can exhibit most excellent properties as an ETL, which makes it possible to realize a high PCE of even above 20 or 21%.

The ambipolar carrier transport properties of the perovskites enabled structural versatility including p–i–n architecture. In the case of p–i–n PSCs, underlying inorganic HTL materials such as NiO, CuO, CuSCN, $MoO_3$, and Cu-based delafossite were applied to the PSCs.[63] The most investigated inorganic HTL in

 

Table 1 Photovoltaic parameters of various ALD-grown CTLs-based PSCs

| Material | Precursor | $T_{substrate}$ (°C) | Device configuration[a] | Device structure | $V_{oc}$ (V) | $J_{sc}$ (mA cm$^{-2}$) | FF (%) | PCE (%) | Ref. |
|---|---|---|---|---|---|---|---|---|---|
| $TiO_2$ | TDMAT + $O_2$ plasma | 150 | nip(P)F | ITO/ALD $TiO_2$/$MAPbI_{3-x}Cl_x$/Spiro-OMeTAD/Au | 0.88 | 14.9 | 0.7 | 9.2 | 45 |
| | TDMAT + $H_2O$ | 80 | nip(M) | FTO/ALD $TiO_2$ nanostructures/$CH_3NH_3PbI_{3-x}Cl_x$/P3HT/Ag | 0.92 | 21.5 | 60.3 | 12.5 | 46 |
| | TDMAT + $H_2O$ | 80 | nio(P) | FTO/ALD $TiO_2$/$CH_3NH_3PbI_{3-x}Cl_x$/P3HT/Ag | 0.98 | 24.3 | 57.1 | 13.6 | 44 |
| | TDMAT + $H_2O$ | 150 | nip(M) | FTO/m-$TiO_2$/ALD $TiO_2$/$MAPbI_3$/Spiro-OMeTAD/Ag | 1.07 | 20.5 | 75.2 | 16.5 | 42 |
| | TDMAT + $H_2O$ | 200 | nip(M) | FTO/ALD $TiO_2$/m-$TiO_2$/perovskite/Spiro-OMeTAD/Au | 0.93 | 18.7 | 72.0 | 12.6 | 43 |
| | TDMAT + $H_2O$ | 120 | nip(P) | FTO/ALD asdep $TiO_2$/$MAPbI_{3-x}Cl_x$/Spiro-PMeTAD/Au | 0.82 | 10.0 | 21.8 | 1.8 | 47 |
| | | 120 | nip(P) | FTO/ALD UV_O3 $TiO_2$/$MAPbI_{3-x}Cl_x$/Spiro-PMeTAD/Au | 0.86 | 25.6 | 45.2 | 10.0 | |
| | | 120 | nip(P) | FTO/ALD 500 °C ann $TiO_2$/$MAPbI_{3-x}Cl_x$/Spiro-PMeTAD/Au | 0.96 | 26.7 | 44.3 | 11.5 | |
| | Ti(CpMe)$(NMe_2)_3$ + $O_2$ plasma | 150 | nip(M)F | PET/ITO/ALD $TiO_2$/m-$TiO_2$/$CH_3NH_3PbI_3$/Spiro-OMeTAD/Au | 1.03 | 17.0 | 75.2 | 13.5 | 41 |
| | Ti(CpMe)$(NMe_2)_3$ + $O_2$ plasma | 150 | nip(P)F | PET/ITO/ALD $TiO_2$/m-$TiO_2$/$CH_3NH_3PbI_3$/Spiro-OMeTAD/Au | 0.86 | 12.1 | 71.9 | 7.5 | 48 |
| | | — | nip(M)F | PET/ITO/ALD $TiO_2$/$CH_3NH_3PbI_3$/Spiro-OMeTAD/Au | 0.91 | 2.9 | 46.7 | 1.3 | |
| | $TiCl_4$ + $H_2O$ | — | nip(P) | FTO/ALD $TiO_2$/$MAPbI_3$/Spiro-OMeTAD/Au | 1.01 | 16.4 | 59.5 | 9.9 | 40 |
| | $TiCl_4$ + $H_2O$ | 300 | nip(M) | FTO/ALD $TiO_2$/m-$TiO_2$/$MAPbI_3$/Spiro-OMeTAD/Ag | 1.02 | 21.0 | 71.9 | 15.4 | 49 |
| | $TiCl_4$ + $H_2O$ | 100 | nip(M) | FTO/ALD $TiO_2$/m-$TiO_2$/$MAPbI_3$/Spiro-OMeTAD/Au | 0.97 | 22 | 68.0 | 11.5 | 38 |
| | TTIP + $O_2$ Plasma | 80 | nip(P)F | PEN/ITO/$CH_3NH_3PbI_{3-x}Cl_x$/Spiro-OMeTAD/Ag | 0.95 | 21.4 | 60.0 | 12.2 | 50 |
| | TTIP + $O_2$ Plasma | 130 | nio(P) | ITO/ALD $TiO_2$/$MAPbI_3$/Spiro-OmeTAD/Au | 1.03 | 20.3 | 75.5 | 15.8 | 51 |
| | TTIP + $H_2O$ | 150 | nip(M) | FTO/ALD $TiO_2$/m-$TiO_2$/$MAPbI_3$/carbon | 0.96 | 19.5 | 41.5 | 7.8 | 52 |
| $SnO_2$ | TDMASn + Ozone | 100 | nip(P) | FTO/c-$TiO_2$/ALD $SnO_2$/$(FAPbI_3)_{0.85}(MAPbBr_3)_{0.15}$/PTAA/Au | 1.13 | 22.7 | 78.0 | 20.0 | 53 |
| | TDMASn + Ozone | 118 | nip(P) | FTO/ALD $SnO_2$/Rb1$(MA_{0.17}FA_{0.83})$99$Pb(I_{0.83}Br_{0.17})_3$/Spiro-OMeTAD/Au | 1.17 | 23.1 | 74.0 | 20.3 | 54 |
| | TDMASn + Ozone | 118 | nip(P) | FTO/ALD $SnO_2$/mixed perovskite/Spiro-OMeTAD/Au | 1.17 | 23.0 | 71.0 | 20.0 | 55 |
| | TDMASn + Ozone | 118 | nip(P) | FTO/ALD $SnO_2$/$(FAPbI_3)_{0.85}(MAPbBr_3)_{0.15}$/Spiro-OMeTAD/Au | 1.14 | 21.3 | 74.0 | 18.4 | 56 |
| | TDMASn + $O_2$ plasma | 100 | nip(P) | FTO/ALD-$SnO_2$/$C_{60}$-SAM/$MAPbI_3$/Spiro-OMeTAD/Au | 1.07 | 20.7 | 70.3 | 15.6 | 57 |
| | TDMASn + $O_2$ plasma | 200 | nip(P) | ITO/ALD $SnO_2$/$Cs_{0.05}(MA_{0.17}FA_{0.83})_{0.95}PbI_{2.7}Br_{0.3}$/Spiro-OMeTAD/Au | 1.08 | 22.1 | 75.0 | 17.8 | 58 |
| | TDMASn + $O_2$ plasma | 100 | nip(P)F | PET/ITO/ALD $SnO_2$/$C_{60}$-SAM/perovskite/Spiro-OMeTAD/Au | 1.10 | 22.1 | 75.4 | 18.4 | 59 |
| | TDMASn + $O_2$ plasma | — | nip(P) | FTO/ALD $SnO_2$/$MA_{0.7}FA_{0.3}PbI_3$/Spiro-OMeTAD/Au | 1.12 | 22.3 | 78.8 | 19.6 | 60 |
| ZnO | $ZnEt_2$ + $H_2O$ | 70 | nip(P) | FTO/450 °C sintered ALD ZnO/$MAPbI_3$/Spiro-OMeTAD/Ag | 0.88 | 11.4 | 59.0 | 6.0 | 61 |
| | $ZnEt_2$ + $H_2O$ | 70 | nip(P) | FTO/ALD ZnO/$MAPbI_3$/Spiro-OMeTAD/Ag | 0.80 | 7.4 | 51.0 | 3.0 | |
| $Nb_2O_5$ | TBTDEN + ozone | 130 | nip(P) | FTO/ALD $Nb_2O_5$/$(FAPbI_3)_{0.85}(MAPbBr_3)_{0.15}$/Spiro-OMeTAD/Au | Very low | | | | 56 |
| NiO | MABONi + ozone | 200 | pin(P) | ITO/ALD NiO/$MAPbI_3$/PCBM/Ag | 1.04 | 21.9 | 72.0 | 16.4 | 35 |
| $TiO_2$–$IrO_x$ | TDMAT/((EtCp)Ir(CHD)) + ozone | 175 | pin(P) | ITO/ALD $TiO_2$–$IrO_x$/$Cs_{0.17}FA_{0.83}Pb(I_{0.83}Br_{0.17})_3$/$C_{60}$/BCP/Ag | 1.01 | 19.6 | 80.0 | 15.8 | 62 |

[a] Device configurations are categorized into nip (regular n–i–p), P (planar heterojunction), M (mesoscopic), F (Flexible), and pin (inverted p–i–n).

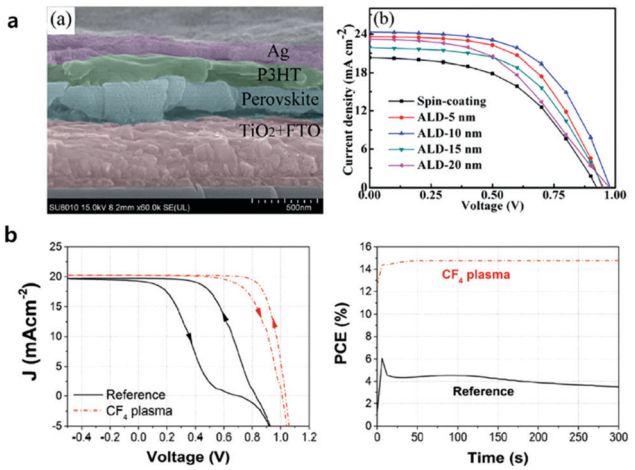


Fig. 4 (a) Cross-sectional SEM image of a perovskite solar cell with FTO/ALD $TiO_2$/perovskite/$P_3HT$/Ag layers and *J*–*V* curves of solar cells based on conventional $TiO_2$ and ALD $TiO_2$ layers (5, 10, 15 and 20 nm). Reproduced with permission.[49] Copyright 2015, The Royal Society of Chemistry. (b) *J*–*V* curves of the perovskite solar cells with ALD $TiO_2$ as the ETL (solid black line) and $CF_4$ plasma-treated ALD (dash red line); and maximum power point tracking (MPPT) for the two devices. Reproduced with permission.[52] Copyright 2018, Wiley-VCH.

p–i–n PSCs is NiO, which requires surface modification, nanostructuring, or doping to minimize its intrinsically high resistances. Seo *et al.* reported the first un-doped pure NiO ultra-thin film *via* ALD in p–i–n PSCs with a PCE of 16.4%.[40] They optimized the thickness of ALD NiO (7.5 nm) and exhibited the appropriated work function of 5.0–5.2 eV and high transmittance of above 95% in the visible range. Tan *et al.* proposed that conventional electron transporting material $TiO_2$ can be a good hole transporting material by the incorporation of $IrO_x$ ($TiO_2$–$IrO_x$ composition *via* super-cycle ALD).[64] This ALD layer has a work function of 5.2 eV and p-type semiconducting property. When 15.5 mol% of $IrO_x$ is incorporated into the $TiO_2$ film, it shows suitable HTL characteristics and a PCE of up to 15.8% at maximum. Several film deposition recipes *via* ALD chemistry were already developed for highly hole conductive CuO, $CuCrO_2$ delafossite, and $MoO_3$, which remained to be demonstrated as highly efficient p–i–n PSCs with these ALD layers.

ETL processed by ALD especially has superiority when applied to tandem or flexible devices requiring low-temperature processes, conformal and pinhole-free films. Albrecht *et al.* realized monolithic Si/perovskite tandem devices *via* low-temperature

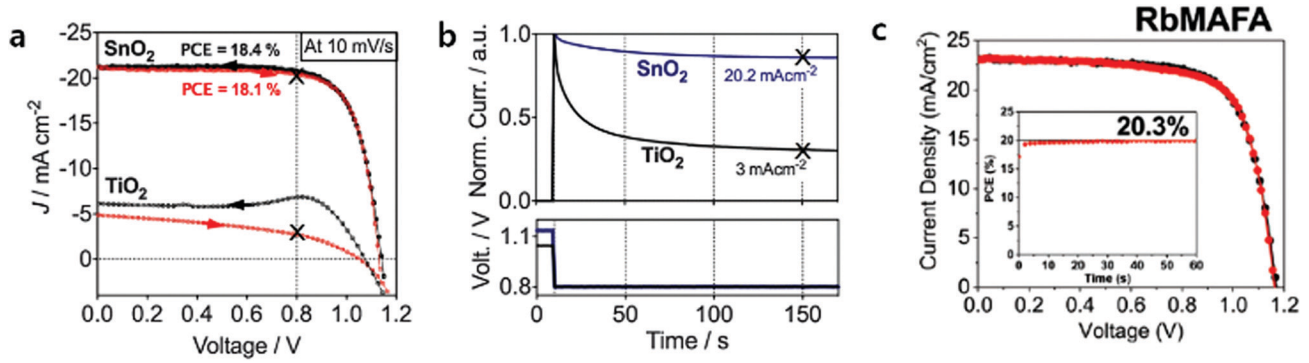


Fig. 5 (a) Current–voltage properties of $TiO_2$ and $SnO_2$-based planar mixed halide/cation perovskite devices. Black arrows indicate the backward scan from $V_{oc}$ to $J_{sc}$, and red arrows indicate the reverse scan. (b) Normalized transient photocurrents measured from the $V_{oc}$ to the maximum power point voltage for both planar systems. Reproduced with permission.[53] Copyright 2015, The Royal Society of Chemistry. (c) The performance of planar PSCs with 1% of Rb in MAFA showed the highest PCE of 20.3%. Reproduced with permission.[13] Copyright 2018, The Royal Society of Chemistry.

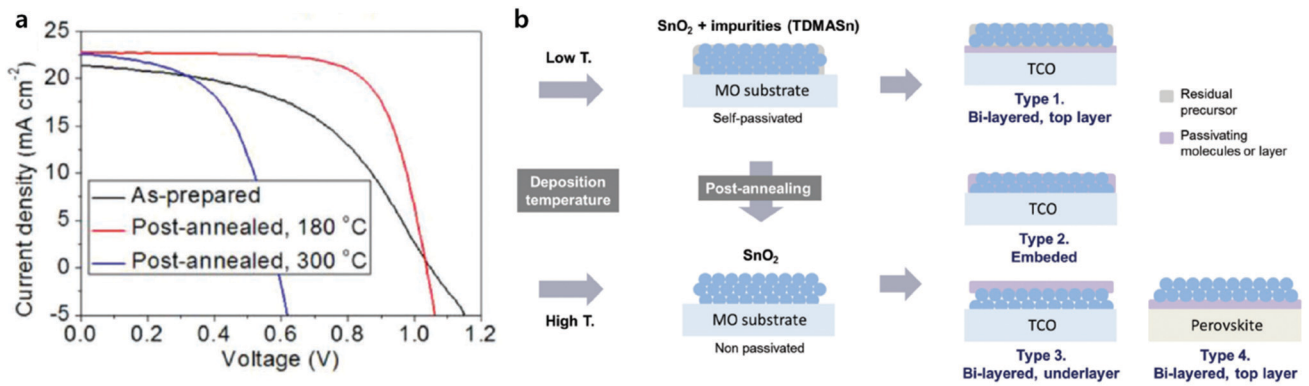


Fig. 6 (a) *J*–*V* curve change according to the post-annealing of ALD $SnO_2$ films. (b) Self- and post-passivation of the ALD $SnO_2$ films. Low-temperature deposition results in incomplete conversion of the precursor, which remains on the $SnO_2$ film as a self-passivating layer. The schematic shows that the surface passivation of $SnO_2$ films can be controlled by post-annealing. Four different methods of post-passivation are proposed. Reproduced with permission.[55] Copyright 2018, The Royal Society of Chemistry.

 

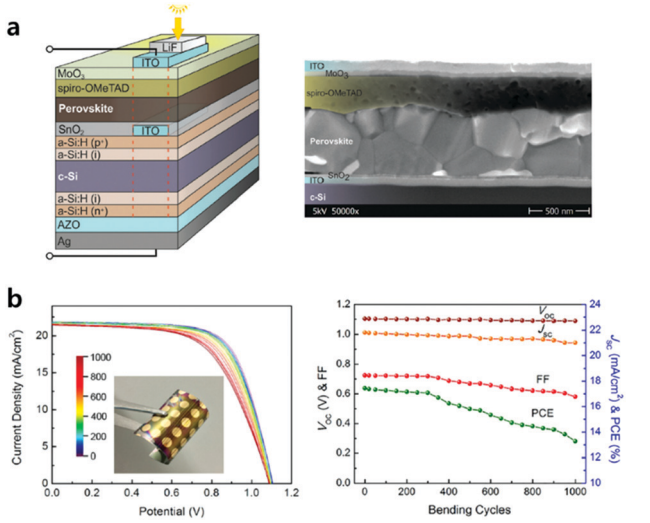


Fig. 7 (a) Schematic of the Si heterojunction/perovskite tandem solar cell (the red dashed line indicates the active area) and cross-sectional scanning electron micrograph of a typical monolithic tandem solar cell. Reproduced with permission.[65] Copyright 2016, The Royal Society of Chemistry. (b) Fatigue testing of a flexible PSC with a bending radius of 1 cm. *J*–*V* curves measured after various bending cycles and performance parameters as a function of bending cycles. Reproduced with permission.[59] Copyright 2017, American Chemical Society.

(118 °C) ALD-processed $SnO_2$ layers (Fig. 7a).[65] They formed a recombination layer of ITO/ALD $SnO_2$ onto the flat Si sub-cell, which functions as an energetically aligned ETL with the perovskite. The ALD ETL in the tandem device is expected to become even more important due to its superior conformality when the Si bottom cell has a textured surface to manage more illuminated light. In the case of flexible devices, ALD $TiO_2$ and $SnO_2$ layers as CTLs were investigated.[49,59,66,67] It is possible to deposit high-quality ETL by ALD at low temperatures (<150 °C), which is required in flexible substrates. It has been also reported that the uniform films without pinholes *via* ALD are more durable against cracks during device bending tests. Wang *et al.* recorded one of the highest PCE (18.36% in the reverse scan direction and a stabilized power output of over 17%) using ALD $SnO_2$ among all n–i–p flexible PSCs.[59] $SnO_2$ *via* plasma-assisted ALD with post-annealing under the water vapour (the entire process at a temperature below 100 °C) showed improved charge transport ability and electrical conductivity. They evidenced that this ALD layer on flexible substrates can alleviate the problems of lower $V_{oc}$, FF and severe current–voltage hysteresis, compared to on rigid substrates. The flexible device retained 76% its initial PCE from 17.4 to 13.3% after 1000 bending cycles (Fig. 7b). They argued that the degradation of flexible ITO/polyethyleneterephthalate (PET) substrates with bending cycles is the predominant reason for the increased sheet resistance and decreased FF and PCE.[68,69]

Another consideration in developing underlying CTLs is the different electronic properties (for example, VB, CB, and work function, *etc.*) of the perovskite films depending on their CTLs, which was reported by several research groups.[70–73] They found that the work function of perovskite films was determined to be around 4.0 eV on n-type substrates (*i.e.*, $TiO_2$, $SnO_2$) while the films were around 4.7 eV for the work function on p-type substrates (*i.e.*, NiO, PEDOT:PSS). Olthof *et al.* proposed that OH– surface groups on oxide materials, by-product formations including the unreacted $PbI_2$ at the surfaces during the film growth, and the interface dipole could be the origin of the different electronic properties of the perovskite films.[71] Hu *et al.* reported a strong impact on the device performance by different $SnO_2$ variants prepared from ALD with three different oxidizers (*i.e.*, $H_2O$, ozone, and plasma-treatment).[70] The device based on ozone $SnO_2$ showed the highest efficiency and $V_{oc}$ of 1.17 V with negligible hysteresis. They asserted that the CB mismatch between the $MAPbI_3$ and the unreacted $PbI_2$ on $SnO_2$ was caused by different interfacial dipoles depending on $SnO_2$ films grown by different oxidizers and surface treatment. A clear understanding of the CTL/perovskite interfaces is still lacking thus far. However, it can be progressed further in the design of efficient PSCs with the understanding of the chemical reactions resulting in the formation of desirable interfaces. For example, the elimination of interfacial $PbI_2$ or control of the interfacial dipole would be viable options to be considered.

### 2.2 Surface passivation/interface engineering

Since the defects and impurities present on the surfaces of the semiconductor promote the electron–hole recombination, interfacial properties of the solar cells are particularly important for highly efficient PVs. Interfaces between the CTLs and perovskite layers are the main source of charge recombination in PSCs.[74] Surface passivation introduced by ultra-thin layers at relatively low temperatures of deposition should cover the surfaces to minimize thermally induced pinholes or cracks in the layers. Thin insulating tunnel layers can also act as a passivation layer by reducing interfacial recombination and charge transfer *via* tunnelling.

ALD provides ideal uniform and conformal passivation films of high quality at a relatively low temperature, which have already been widely adopted as a passivation layer in other solar cell fabrication processes.[75] Chandiran *et al.* proposed the nanometer-thickness ALD $TiO_2$ overlayers (0–4 nm) on mesoporous $TiO_2$-based PSCs to suppress electron recombination, leading to a PCE of 11.5% without further heat treatment.[76] Similar concepts of ALD metal oxide passivation films with the thickness of few nanometres have been employed in various configurations (ALD ZnO on mesoporous $Al_2O_3$,[77] ALD $Al_2O_3$ between FTO/mesoporous $TiO_2$,[78] ALD $TiO_2$ on 1-D nanorod $TiO_2$,[79] *etc.*[76,80,81]).

The passivation process on the TCO electrodes or TCO/metal oxide substrates before perovskite coating is more challenging and limited than the passivation process on top of the perovskite or perovskite/CTLs in terms of compatibility without having any damage underneath the perovskite layers, prone to degradation, during the process.[82] However, when the passivation process over the perovskite is performed successfully, the passivation layer can not only reduce charge recombination at the interface but also improve the stability of the perovskite by protecting the degradation reaction with moisture and/or oxygen from outside of the cells. Dong *et al.* investigated ultrathin $Al_2O_3$ prepared by ALD on the perovskite layer as a passivation process.[83]

They deposited $Al_2O_3$ directly onto the perovskite using TMA and $O_3$ with a relatively low temperature of 70 °C to avoid the thermally induced degradation of the perovskite and organic HTL. The perovskite was degraded even after 1 cycle of the ALD process, which resulted in the reduced performance of the PSCs. Even though they reported the successful enhancement of stability by adopting the $Al_2O_3$ layer, they did not explain the passivation tunnelling effect of ALD $Al_2O_3$ due to the performance drop. Kim *et al.* proposed novel ALD chemistry of the non-hydrolytic process using carboxyl acid as an oxidizer for $Al_2O_3$ deposition to avoid perovskite degradation.[84] They were not successful in showing PSCs adopting the non-hydrolytic ALD process, due to which the passivation effect of the film remains unclarified.

Recently, Koushik *et al.* deposited 2–20 cycles of ALD $Al_2O_3$ onto the perovskite at room temperature without degradation, evidenced by the X-ray diffraction (XRD) spectra as shown in Fig. 8.[85] The thickness of the $Al_2O_3$ films was grown conformally and precisely controlled at the Angstrom scale by varying the number of ALD cycles. Devices without $Al_2O_3$ layers exhibited a PCE of 15.1%. Device passivated by $Al_2O_3$ showed considerable improvement in all PV performances with sub-optimal conditions (2–8 cycles) and optimal conditions (10–15 cycles). Further increasing the number of ALD cycles over 15 resulted in a significant decrease in the $J_{sc}$ and FF. The author addressed that the relatively thick $Al_2O_3$ worsened the tunnelling effect, followed by less probable hole injection from the perovskite to the HTL. ALD $Al_2O_3$ layers with an optimal thickness (10 cycles ~1 nm) positively affected current–voltage hysteresis and increased the PCE of PSCs up to 18%, which provided sufficient tunnelling passivation effect and protected the underneath perovskite layers. 70 days of dark aging under a stepwise increasing humidity (RH 40% to 70%) demonstrated that the $Al_2O_3$ passivation layers delay humidity-induced degradation, as it retained 70% of its initial efficiency, while devices without the $Al_2O_3$ layers lost almost all highly efficient PV performance.

Hu *et al.* reported another passivation material, *i.e.*, ALD $ZrO_2$ to modify the interface between perovskite/PCBM in $MAPbBr_3$-based inverted planar PSCs.[86] Hole blocking by $ZrO_2$ suppresses charge recombination loss and consequently produces a remarkably high $V_{oc}$ of 1653 mV. The author additionally addressed the origin of $V_{oc}$ enhancement of $ZrO_2$-inserted PSCs, since the arrangement of PCBM films is more ordered on the perovskite/$ZrO_2$ surface, as evidenced by XRD analysis.

### 2.3 Overlying ETL *via* ALD for stability engineering

The stability of PSCs for the goal of commercially available products is one of the most difficult challenges in PSCs. The prototypical light absorbing material in PSCs is $CH_3NH_3PbI_3$, which has $ABX_3$ perovskite crystal structure, and it has a relatively low lattice formation energy of −29.71 eV per cell, as much as 1-order of magnitude lower than typical oxide perovskites, resulting in facile degradation under moisture, oxygen, heat, electrical bias, as well as from light illumination.[87] It has been proposed that alternating or mixing the A-site elements of MA with formamidinium (FA), Cs, Rb or even bigger organic cations to

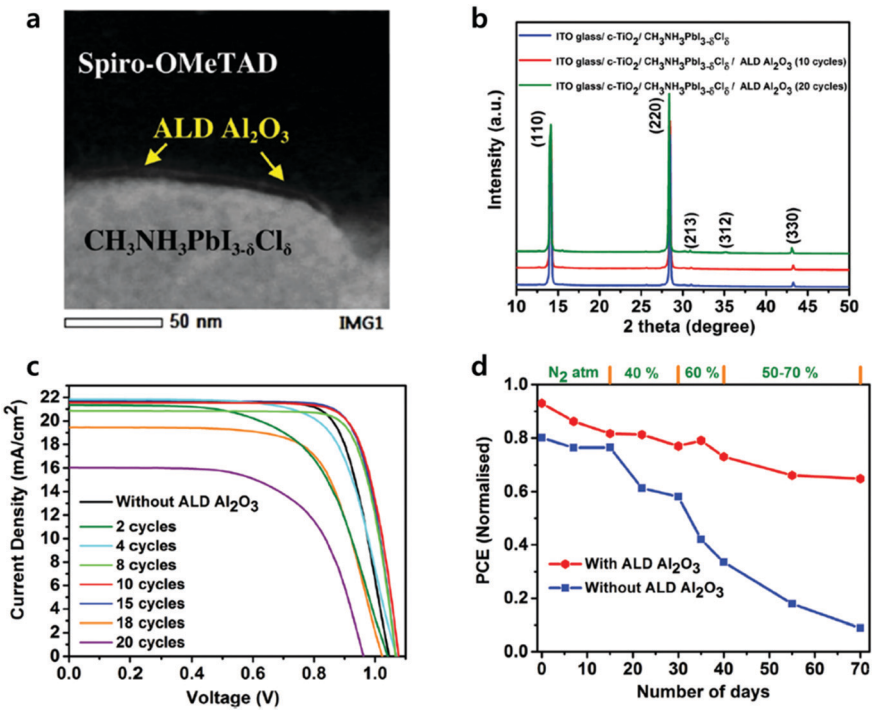


Fig. 8 (a) High-angle annular dark field (HAADF) scanning TEM image of the enlarged perovskite/ALD $Al_2O_3$/Spiro-OMeTAD interface. (b) XRD spectra of the parent perovskite film before and after the successive depositions of ALD $Al_2O_3$. (c) *J*–*V* curves of the best perovskite devices utilizing different numbers of ALD $Al_2O_3$ cycles. (d) Normalized PCE of the champion perovskite devices with and without ALD $Al_2O_3$ as a function of storage time under varied humidity conditions. Reproduced with permission.[85] Copyright 2017, The Royal Society of Chemistry.

 

enhance the lattice formation energy can stabilize the perovskite structure and eventually increased the stability of the devices.

Asghar *et al.* reviewed the understanding of the degradation mechanisms of PSCs originated from all the device components from the perovskite, transport layers, electrodes, and device geometry.[88] Not to mention the stability of the perovskite material itself, other components can promote or retard the degradation of PSCs. The components on top of the perovskite are of particular interest due to the additional protecting role preventing the penetration of moisture from the outside and its own stability. The conventional HTL in regular-type PSCs is the Spiro-OMeTAD, PTAA and poly(3-hexylthiophene) (P3HT), which is solution-processed. Yang *et al.* studied the ability of HTL to prevent moisture-induced degradation onto the perovskite.[89] They found that Spiro-OMeTAD causes an acceleration of the decomposition of the perovskite due to the HTL undergoing significant cracking, while other HTLs show a reduction in the degradation rates. They explained the different rates of perovskite decomposition by the toughness of the layer. PCBM, the most common ETL in inverted devices, has been reported to inhibit water permeation due to its hydrophobic nature.[90] Thus, this is the reason why layers over the perovskite should be dense, impermeable and free of pinholes in terms of stability.

ALD has been proposed as a promising method to produce an excellent protective layer when deposited onto the perovskite layer.[84] Metal oxide films were grown *via* ALD with great impermeability originating from dense, conformal, and pinhole-free nature with an extremely low water vapour transmission rate (WVTR).[91] The first application of ALD for stable PSCs was reported by depositing a few cycles of $Al_2O_3$ directly onto the perovskite layer as introduced in the previous passivation section.[92]

In spite of its sub-nanometer thickness, it has improved the atmospheric air stability of PSCs. The trade-off between stability and charge transfer occurs simply because the thick film demonstrated sufficient impermeability, while charge transfer *via* tunnelling is severely suppressed. In order to avoid this problem, the deposition of 10–20 nm of ALD ETLs onto the perovskite-PCBM heterojunction has been proposed. ALD ETLs functions as a protective layer as well as CTLs in the inverted p–i–n type PSCs. Table 2 shows important stability results based on ALD ETL adopted inverted PSCs reported in the literature.[91,93–97] The direct deposition of an ALD ETL with a thickness over 10 nm onto the perovskite usually decomposes the perovskite vigorously during the process, which make the final PCE less than 10%.[98,99]

Kim *et al.* prepared $TiO_2$ layers by ALD in the inverted PSCs, which showed remarkable improvement in resistance against degradation in harsh environments such as soaking in liquid water or high temperatures (100 °C).[93] It has also been reported by Brinkmann *et al.* that 20 nm thick impermeable ALD-$SnO_2$ ETLs can suppress the decomposition of the perovskite.[94] PSCs with ALD-$SnO_2$ preserved their performance (~12%) during 500 hours of dark storage under humid atmospheric exposure (relative humidity (RH) of 50%) without any sign of degradation, while PSCs without the $SnO_2$ layer degraded rapidly within 50 hours. They analysed the reason why $SnO_2$-inserted PSCs showed strikingly high stability, as shown in Fig. 9. From the XRD data, they found no severe decomposition of the perovskite when exposed to moisture regardless of $SnO_2$ deposition, which meant that the bulk of the perovskite remained unchanged. On the other hand, XPS results showed a notable degradation with increasing $I_3d_{5/2}$ binding peaks from AgI on the surface of devices without ALD $SnO_2$. Similar XPS analysis of thermally aged (60 °C) samples showed consistent results that the ALD $SnO_2$ layer successfully prevented the evaporation of volatile organic components (*e.g.*, MAI). They claimed that outstandingly dense gas permeation barriers by ALD suppressed the out-diffusion of the decomposition products.

The moisture-induced degradation of PSCs can be overcome by proper encapsulation of the devices. Typical metal electrodes, such as Ag and Au, can diffuse through the organic transport layers and make detrimental reactions with the perovskite layers at the interface under operational condition or at high temperatures.[100] Aforementioned ALD-grown inorganic CTLs are critical to prevent roles against in-/out-diffusion. Guerrero *et al.* reported the interfacial degradation of PSCs, as shown in Fig. 10a.[101] PSCs under operational conditions including the light and electric field generate ion migration inside perovskite films, leaving the accumulation of net charges at one or both contacts. Light and electric field-driven chemical reaction by the diffusion of these ions and metals cause interfacial degradation between the perovskite/PCBM and the PCBM/metal, which finally induced a severe drop of the PCE even under inert atmosphere.

Table 2 Accelerated aging tests results for inverted PSCs based on impermeable ETLs. Devices are completed with ALD metal oxide on the perovskite-PCBM heterojunction. Stability results indicate the retained performance after each aging condition

| ALD metal oxide | Device structure | PCE (%) | Ageing condition and stability results | Ref. |
|---|---|---|---|---|
| ZnO | ITO/PEDOT:PSS/$MAPbI_3$/PCBM/ALD ZnO/Ag NWs/50 nm $Al_2O_3$ coated PET | 10.8 | Dark storage in ambient air ~95% retaining for 42 days | 87 |
| $TiO_2$ | ITO/$NiO_x$/$MAPbI_3$/PCBM/ALD $TiO_2$/Al/Au | 8.8 | Dark storage under thermal soaking (100 °C) 91% retaining for 10 hours | 88 |
| $SnO_2$ | ITO/PEDOT:PSS/$MAPbI_3$/PCBM/Al:ZnO/ALD $SnO_2$/Ag | 12.6 | Dark storage in 23 °C and 50% RH or inert under 60 °C no degradation | 89 |
| $SnO_2$ | ITO/PEDOT:PSS/$MAPbI_3$/PCBM/Al:ZnO/ALD $SnO_2$/Ag/$SnO_2$ | 11.2 | Dark storage in inert 60 °C 95% retaining for 3200 hours | 90 |
| $SnO_2$ | ITO/PEDOT:PSS/$MAPbI_3$/PCBM/Al:ZnO/spatial ALD $SnO_2$/Ag | 12.7 | Dark storage in 23 °C and 60% RH ~92% retaining for 1000 hours | 91 |
| Al:ZnO | FTO/NiO/$MAPbI_3$/PCBM/BCP/ALD-Al:ZnO/Ag/$Al_2O_3$(90 nm) | 18.5 | 85 °C, 1 sun illumination, ambient air, MPPT 86.7% retaining for 500 hours | 92 |

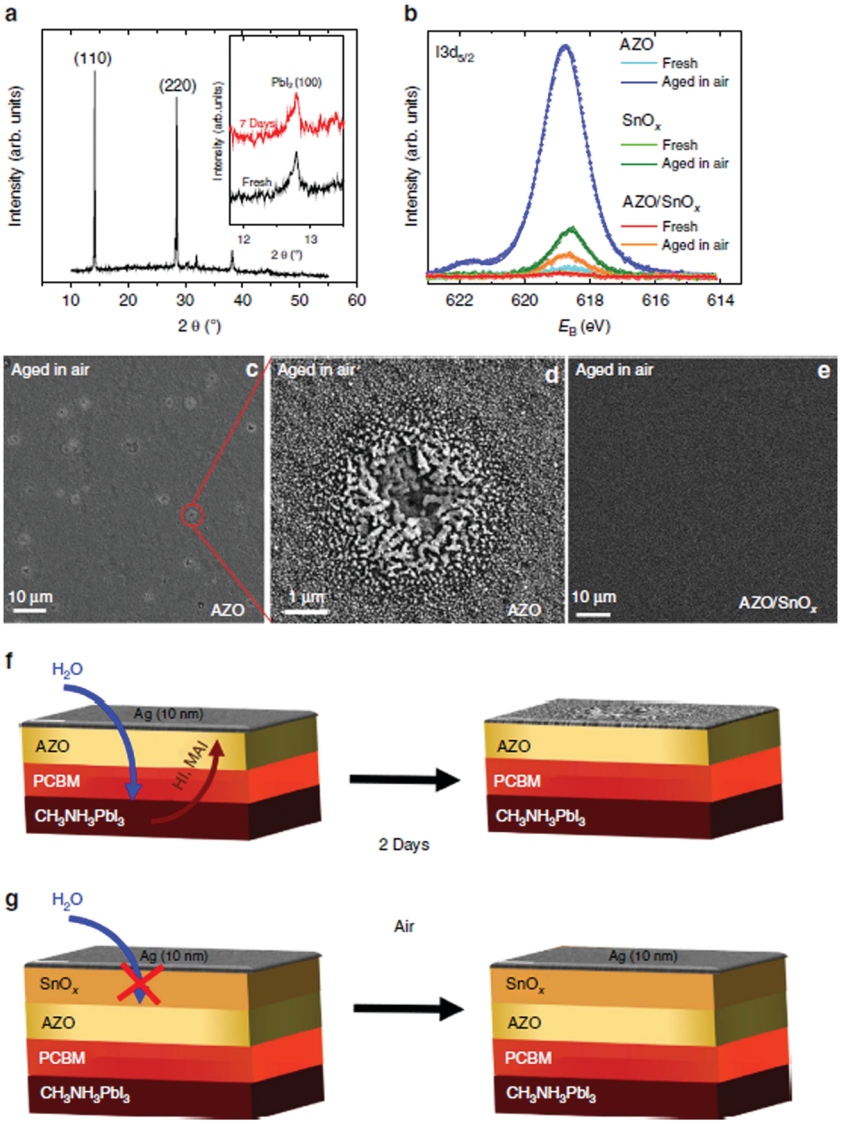


Fig. 9 Unravelling the aging mechanism in air. XRD spectrum of a perovskite cell based on AZO as ETL after storage in air for 7 days (inset: magnified view of the (100) $PbI_2$ reflection for a fresh sample and one that has been stored in air for 7 days; spectra were vertically offset for clarity) (a). Photoemission spectra of the iodine $I_3d_{5/2}$ peak for fresh and aged cells based on AZO, $SnO_x$ and bilayered AZO/$SnO_x$ ETLs, respectively (b). The aged samples were stored in air for 2 days. Corresponding plan-view SEM images of the 10 nm Ag layer in the case of the AZO sample (c and d), and for the AZO/$SnO_x$ sample (e). Schemes of the aging for the AZO and the AZO/$SnO_x$ samples (f and g). Reproduced with permission.[94] Copyright 2016, Macmillan Publishers Limited.

Seo *et al.* rationalized the use of the dense ALD-ETL layer between perovskite/PCBM and metal electrodes by suppressing interfacial degradation, as shown in Fig. 10b and c.[97] They fabricated inverted PSCs using ALD Al:ZnO with FTO/NiO/perovskite/PCBM/Al:ZnO/Ag. Al:ZnO-adopted PSCs exhibited 17% efficiency, which produced similar device performance to the control device without Al:ZnO due to the negligible charge transporting retardation by the 3 orders of magnitude higher conductivity of Al:ZnO compared to that of PCBM. Regarding the stability of PSCs, while the control solar cells have been degraded rapidly under continuous 1 sun light illumination at room temperature in spite of the additional encapsulation layer (90 nm of $Al_2O_3$), Al:ZnO PSCs maintained almost all of its initial efficiency. The author addressed that the unique role of Al:ZnO, distinguished from other encapsulation techniques, is to prevent moisture penetration as well as interdiffusion at the perovskite/Ag interface when illuminated. The Al:ZnO layer prevents interfacial degradation between the perovskite-heterojunction and the Ag electrode caused by unfavourable chemical reaction. These perovskite solar cells demonstrated their stability in a harsher environment, exhibiting a power conversion efficiency of 18.45% and retaining 86.7% of its initial efficiency for 500 hours under continuous 1 sun illumination at 85 °C in ambient air with electrical biases (at the maximum power point). The application of the ALD ETL over the perovskite layer has another function of extending process compatibility to prevent deterioration of the perovskite during the deposition of transparent electrodes such as ITO. It was proposed by Bush *et al.* that sputtered ITO was

 

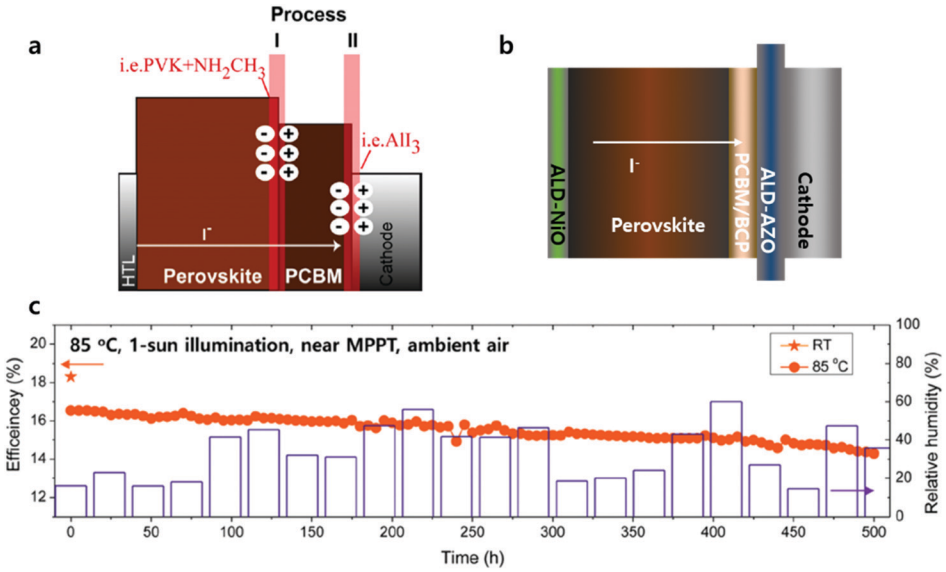


Fig. 10 (a) Feasible hypothesis that could potentially give rise to external cathode contact degradation. Reproduced with permission.[101] Copyright 2015, American Chemical Society. (b) Schematic of PSCs with suppressed interfacial degradation in the presence of the ALD Al:ZnO layer. (c) PCE evolution of the ALD-Al:ZnO-coated PSC with a thin $Al_2O_3$ passivation film (≈50 nm) over 500 h. Aging was performed under continuous near maximum power electrical biases (0.76–0.88 V) and 1 sun illumination (100 mW $cm^{-2}$) with a 420 nm cutoff UV filter at 85 °C in ambient air (the relative humidity was ≈20–60%). The relative humidity was recorded every day. The initial PCE value (orange star) was 18.4% at room temperature, and the PCE at 85 °C (orange circles) was recorded every 5 h. The ALD-Al:ZnO-coated device retained 86.7% of its initial performance (16.5% → 14.3%), as determined from the reverse *J*–*V* scan. Reproduced with permission.[97] Copyright 2018, Wiley-VCH.

successfully able to complete semi-transparent PSCs in the presence of ALD ETL due to its impermeability minimizing sputtered damage onto the perovskite.[102] Moreover, Snaith and co-workers recently fabricated a solution-processed perovskite–perovskite tandem solar cell by utilizing ALD $SnO_2$ as a buffer layer for the ITO sputtering process.[102,103] The intermittent layer ($SnO_2$/ITO) successfully protects underneath the perovskite during the top cell fabrication process.

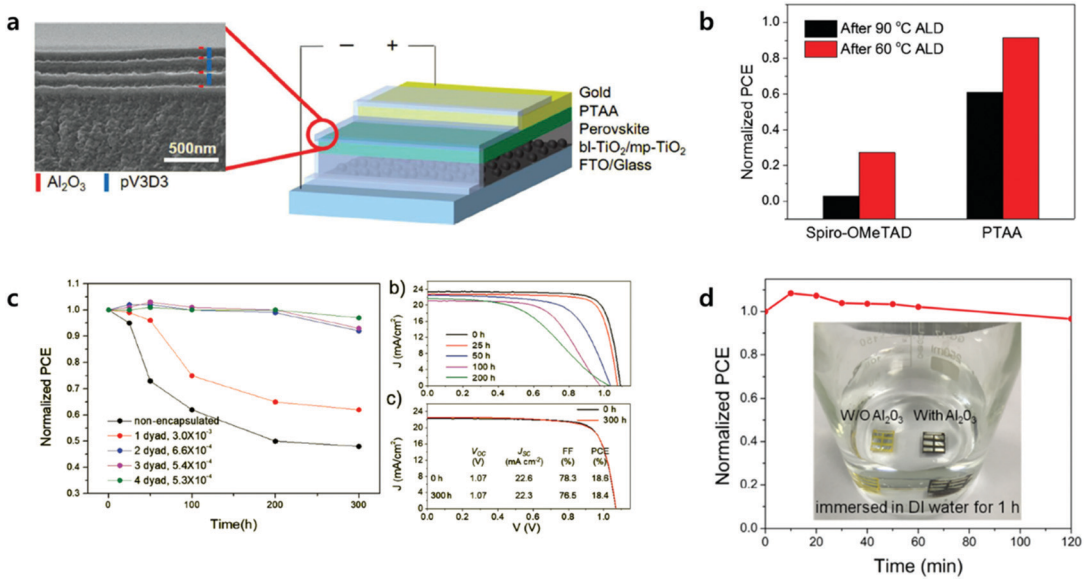


Fig. 11 (a) Right: Schematic of the encapsulated PSC. Left: The cross-sectional SEM image of the TFE. (b) Normalized PCE of HTM-varied PSCs after 60 and 90 °C ALD processes. (c) Shelf life of PSC encapsulated with 1–4 layers of multilayer TFE under an accelerated condition of 50 °C, 50% RH. The numbers in legend indicate the WVTR of each TFE (g $m^{-2}$ $d^{-1}$). *J*–*V* characteristics of (b) pristine PSC and (c) PSC encapsulated with 4-dyad TFE with respect to time lapse under reverse scan. Reproduced with permission.[107] Copyright 2017, Wiley-VCH. (d) Evolution of normalized PCE for $Al_2O_3$-protected devices immersed in water. The inset shows photographs of the devices with $Al_2O_3$ (right) and without $Al_2O_3$ (left) layers after being kept in water for 1 h. Reproduced with permission.[109] Copyright 2018, American Chemical Society.

### 2.4 Encapsulation *via* ALD

The key factor in achieving long-term stable PSCs is largely related to developing stable perovskite materials and/or device architectures including encapsulation. Encapsulation methods are utilized extensively in organic PVs (OPVs) or organic light emitting diodes (OLEDs), which requires levels of WVTR less than $10^{-6}$ g m$^{-2}$ d$^{-1}$ for long-lived OLEDs.[104] However, encapsulation technology with adequate WVTR levels has not been developed yet in PSCs due to them being prone to the degradation of perovskite materials during the encapsulation processes.[105,106]

Lee *et al.* reported the first laminated (inorganic and organic stacked layers) encapsulation thin film (thickness of less than 5 μm) for the encapsulation of PSCs, composed of pairs of $Al_2O_3$ and poly(1,3,5-trimethyl-1,3,5-trivinylcyclotrisiloxane) ($pV_3D_3$) processed by ALD and iCVD, respectively. Four pairs of $Al_2O_3$ and $pV_3D_3$ display an outstanding barrier property of $10^{-4}$ g m$^{-2}$ d$^{-1}$ of WVTR under a high RH of 90% and 38 °C.[107] Fig. 11 shows the effect of the ALD process temperature on the performance of the PSCs. In the case of PSCs with PTAA as the HTL, the performance retained 90% of its initial efficiency after the ALD process at 60 °C. One pair of $Al_2O_3$ and $pV_3D_3$ encapsulation films do not cause much deterioration of the performance, changing from 21.5 to 20.1%. PSCs with 4 pairs of encapsulation films maintained 97% of their initial PCE for 300 hours of ageing under 50 °C/50% (temperature/RH). The longest shelf life of PSCs, with an efficiency greater than 18%, has been achieved.

Unlike regular PSCs, inverted PSCs usually showed better thermal stability due to the presence of PCBM instead of spiro-OMTeAD.[91,108] The ALD $Al_2O_3$ process below 100 °C does not significantly affect the performance of inverted PSCs. Lv *et al.* reported a composite ALD $Al_2O_3$ encapsulation layer in multi-layers composed of $Al_2O_3$ (10 nm)/$Al_2O_3$ with intermediates of the Al precursor (20 nm)/$Al_2O_3$ (30 nm) processed at 60 °C.[109] PSCs with the $Al_2O_3$ multilayer showed great water resistance, retaining 95% of the initial efficiency after 2 hours of being immersed in DI water, as shown in Fig. 11d. Thin $Al_2O_3$ layers do not exhibit ideal water resistance at all. Water molecules might penetrate the layers from the surface of the $Al_2O_3$ up to the perovskite layers very slowly by forming H bonds with oxygens and migrating the species. They also proposed the novel concept of retarding water penetration. Intermediates of the Al precursor layer (O–Al–$(CH_3)_{3-x}$), between the top and bottom dense $Al_2O_3$ layers, additionally react with water. The intermediate layer can be converted into compact $Al_2O_3$ layers, which significantly decrease the overall water penetration rates as well as eliminating invading water molecules.

## 3. Conclusions

In this review, we mainly focused on underlying CTLs as well as overlying perovskite layers, surface passivation layers, and encapsulating layers all deposited by ALD in PSCs. A reduction of the thickness of CTLs can reduce the device serial resistance. Processing such ultra-thin films, however, has been challenging, and most thin film processing resulted in pinholes and cracks, leading to reduced charge carrier blocking ability and creating a shunt leakage pathway. Furthermore, in the case of large area substrates and/or substrates with a high-aspect ratio, the formation of ultra-thin films with uniform thicknesses is even more challenging. ALD can produce ideal CTLs with conformal and dense film growth with precise sub-nanometer scale thickness control. ETL processed by ALD has superiority when applied to tandem or flexible devices requiring low-temperature processes, conformal and pinhole-free films. ALD has also been widely adopted as a passivation layer in many different solar cell fabrication processes. Unlike passivation processed on the TCO electrodes or TCO/metal oxide substrates before perovskite coating, it is more challenging and limited than the passivation process atop of perovskite or perovskite/CTLs in terms of compatibility without having any damage underneath perovskite layers, prone to degradation. However, when the passivation process over the perovskite is performed successfully, the passivation layer can not only reduce charge recombination at the interface but also improve the stability by protecting the degradation reaction with moisture and/or oxygen from the outside. ALD has been proposed as a promising method to produce an excellent protective layer when deposited onto the perovskite layer. Metal oxide films grown *via* ALD, having great impermeability originating from a dense, conformal, and pinhole-free nature with extremely low water vapour transmission rate, can be a solution for the commercialization in PSCs.

Further efficiency improvement can be expected in PSCs based on ALD CTLs by developing other potential candidate materials such as $WO_3$, $MoO_3$, $V_2O_5$, $CuO_x$, doping strategies and interfacial engineering. Considering that many doping chemistries using ALD have already been reported, it would be an effective way to produce highly efficient CTLs. Until now, applications of doped CTLs *via* ALD for PSCs have rarely been reported. Furthermore, it is still unclear why perovskite layers exhibit different electronic properties depending on CTLs and their surface states. Since ALD can provide the same material with different surface properties using various oxidizers under similar growth conditions, it would be an ideal model system to understand the interfacial property between CTLs and perovskites.

The newly developed ALD ETL overlying perovskite has demonstrated huge potential for the stability improvement of PSCs. However, all these works have been directed towards inverted-type PSCs with $MAPbI_3$. Thermally and chemically more stable perovskites containing Cs, FA, Rb, and/or Br will be able to explore the new possibility of the direct deposition of ETLs onto the perovskite layer without PCBM, which can reduce device serial resistance and complexity while preserving the efficiency of PSCs. Moreover, considering the overall efficiencies of regular-type PSCs, exhibiting higher PCEs compared to inverted-type PSCs, the development of ALD HTL overlying perovskite would be promising in terms of improving device stability as well as efficiency. Encapsulations *via* ALD $Al_2O_3$ for PSCs have been reported in the limited number of research papers to date. It is remarkable that negligible degradation in PV performance with encapsulation has been observed. It is also necessary to further reduce the WVTR of encapsulation layers for

 

PSCs by benchmarking the excellent ALD encapsulation technology (*e.g.* $ZrO_2/Al_2O_3$ bi-layer,[110] organic/inorganic multilayer[104]) already developed in other fields. ALD techniques show great potential for efficient and stable PSCs and in the future will become the most viable ones in the fabrication of commercial PSCs.

## Conflicts of interest

There are no conflicts to declare.

## Acknowledgements

The authors acknowledge the Ministry of Science, ICT & Future Planning (MSIP) of Korea under contracts with NRF-2017R1A4A1015770 (Basic Research Laboratory Program), NRF-2016M3D1A1027664 (Future Materials Discovery Program), NRF-2018K1A3A1A32055268 and NRF-2018M3C1B7021994 through the National Research Foundation of Korea (NRF).

## Notes and references

1 A. Kojima, K. Teshima, Y. Shirai and T. Miyasaka, *J. Am. Chem. Soc.*, 2009, **131**, 6050.
2 J. H. Im, C. R. Lee, J. W. Lee, S. W. Park and N. G. Park, *Nanoscale*, 2011, **3**, 4088.
3 H. S. Kim, C. R. Lee, J. H. Im, K. B. Lee, T. Moehl, A. Marchioro, S. J. Moon, R. Humphry-Baker, J. H. Yum, J. E. Moser, M. Gratzel and N. G. Park, *Sci. Rep.*, 2012, **2**, 591.
4 L. Etgar, P. Gao, Z. S. Xue, Q. Peng, A. K. Chandiran, B. Liu, M. K. Nazeeruddin and M. Gratzel, *J. Am. Chem. Soc.*, 2012, **134**, 17396.
5 M. M. Lee, J. Teuscher, T. Miyasaka, T. N. Murakami and H. J. Snaith, *Science*, 2012, **338**, 643.
6 H. J. Snaith, *J. Phys. Chem. Lett.*, 2013, **4**, 3623.
7 Q. Q. Lin, A. Armin, P. L. Burn and P. Meredith, *Acc. Chem. Res.*, 2016, **49**, 545.
8 J. P. Correa-Baena, A. Abate, M. Saliba, W. Tress, T. J. Jacobsson, M. Gratzel and A. Hagfeldt, *Energy Environ. Sci.*, 2017, **10**, 710.
9 J. S. Manser, J. A. Christians and P. V. Kamat, *Chem. Rev.*, 2016, **116**, 12956.
10 Y. X. Zhao and K. Zhu, *Chem. Soc. Rev.*, 2016, **45**, 655.
11 M. A. Green and A. Ho-Baillie, *ACS Energy Lett.*, 2017, **2**, 822.
12 B. R.-C. National Renewable Energy Laboratory and E. c. https://www.nrel.gov/pv/assets/images/efficiency-chart.png.
13 H. R. Tan, A. Jain, O. Voznyy, X. Z. Lan, F. P. G. de Arquer, J. Z. Fan, R. Quintero-Bermudez, M. J. Yuan, B. Zhang, Y. C. Zhao, F. J. Fan, P. C. Li, L. N. Quan, Y. B. Zhao, Z. H. Lu, Z. Y. Yang, S. Hoogland and E. H. Sargent, *Science*, 2017, **355**, 722.
14 W. S. Yang, B. W. Park, E. H. Jung, N. J. Jeon, Y. C. Kim, D. U. Lee, S. S. Shin, J. Seo, E. K. Kim, J. H. Noh and S. I. Seok, *Science*, 2017, **356**, 1376.
15 X. Zheng, B. Chen, J. Dai, Y. Fang, Y. Bai, Y. Lin, H. Wei, X. C. Zeng and J. Huang, *Nat. Energy*, 2017, **2**, 17102.
16 D. Bi, C. Yi, J. Luo, J.-D. Décoppet, F. Zhang, S. M. Zakeeruddin, X. Li, A. Hagfeldt and M. Grätzel, *Nat. Energy*, 2016, **1**, 16142.
17 Q. Jiang, Z. Chu, P. Wang, X. Yang, H. Liu, Y. Wang, Z. Yin, J. Wu, X. Zhang and J. You, *Adv. Mater.*, 2017, **29**, 1703852.
18 Z.-L. Tseng, C.-H. Chiang, S.-H. Chang and C.-G. Wu, *Nano Energy*, 2016, **28**, 311.
19 S. S. Shin, W. S. Yang, J. H. Noh, J. H. Suk, N. J. Jeon, J. H. Park, J. S. Kim, W. M. Seong and S. I. Seok, *Nat. Commun.*, 2015, **6**, 7410.
20 S. S. Shin, E. J. Yeom, W. S. Yang, S. Hur, M. G. Kim, J. Im, J. Seo, J. H. Noh and S. I. Seok, *Science*, 2017, **356**, 167.
21 W. Chen, Y. Wu, Y. Yue, J. Liu, W. Zhang, X. Yang, H. Chen, E. Bi, I. Ashraful, M. Grätzel and L. Han, *Science*, 2015, **350**, 944.
22 C. Zuo and L. Ding, *Small*, 2015, **11**, 5528.
23 S. Ye, H. Rao, Z. Zhao, L. Zhang, H. Bao, W. Sun, Y. Li, F. Gu, J. Wang, Z. Liu, Z. Bian and C. Huang, *J. Am. Chem. Soc.*, 2017, **139**, 7504.
24 P.-L. Qin, H.-W. Lei, X.-L. Zheng, Q. Liu, H. Tao, G. Yang, W.-J. Ke, L.-B. Xiong, M.-C. Qin, X.-Z. Zhao and G.-J. Fang, *Adv. Mater. Interfaces*, 2016, **3**, 1500799.
25 H. Zhang, H. Wang, W. Chen and A. K.-Y. Jen, *Adv. Mater.*, 2017, **29**, 1604984.
26 P.-L. Qin, Q. He, C. Chen, X.-L. Zheng, G. Yang, H. Tao, L.-B. Xiong, L. Xiong, G. Li and G.-J. Fang, *Sol. RRL*, 2017, **1**, 1700058.
27 H. Zhang, H. Wang, H. Zhu, C.-C. Chueh, W. Chen, S. Yang and A. K.-Y. Jen, *Adv. Energy Mater.*, 2018, **8**, 1702762.
28 F. Hou, Z. Su, F. Jin, X. Yan, L. Wang, H. Zhao, J. Zhu, B. Chu and W. Li, *Nanoscale*, 2015, **7**, 9427.
29 K. M. Deng and L. Li, *Adv. Mater. Interfaces*, 2016, **3**, 1600505.
30 V. Zardetto, B. L. Williams, A. Perrotta, F. Di Giacomo, M. A. Verheijen, R. Andriessen, W. M. M. Kessels and M. Creatore, *Sustainable Energy Fuels*, 2017, **1**, 30.
31 R. L. Puurunen, *Chem. Vap. Deposition*, 2014, **20**, 332.
32 V. Miikkulainen, M. Leskela, M. Ritala and R. L. Puurunen, *J. Appl. Phys.*, 2013, **113**, 021301.
33 W. B. Niu, X. L. Li, S. K. Karuturi, D. W. Fam, H. J. Fan, S. Shrestha, L. H. Wong and A. L. Y. Tok, *Nanotechnology*, 2015, **26**, 13.
34 L. Ma, R. B. Nuwayhid, T. P. Wu, Y. Lei, K. Amine and J. Lu, *Adv. Mater. Interfaces*, 2016, **3**, 1600564.
35 Y. Widjaja and C. B. Musgrave, *Appl. Phys. Lett.*, 2002, **80**, 3304.
36 S. Lee, C. Bae and H. Shin, *ACS Appl. Mater. Interfaces*, 2018, **10**, 20929.
37 S. Lee, C. Bae, J. Lee, S. Lee, S. H. Oh, J. Kim, G. S. Park, H. S. Jung and H. Shin, *Adv. Mater.*, 2018, **30**, 1706261.
38 H. Shin, D. K. Jeong, J. Lee, M. M. Sung and J. Kim, *Adv. Mater.*, 2004, **16**, 1197.
39 M. D. Groner, F. H. Fabreguette, J. W. Elam and S. M. George, *Chem. Mater.*, 2004, **16**, 639.
40 S. Seo, I. J. Park, M. Kim, S. Lee, C. Bae, H. S. Jung, N. G. Park, J. Y. Kim and H. Shin, *Nanoscale*, 2016, **8**, 11403.
41 T. A. Ho, C. Bae, S. Lee, M. Kim, J. M. Montero-Moreno, J. H. Park and H. Shin, *Chem. Mater.*, 2017, **29**, 7604.
42 H. Nam, C. Bae and H. Shin, *ChemistrySelect*, 2018, **3**, 11027.
43 K. E. Roelofs, V. L. Pool, D. A. Bobb-Semple, A. F. Palmstrom, P. K. Santra, D. G. Van Campen, M. F. Toney and S. F. Bent, *Adv. Mater. Interfaces*, 2016, **3**, 1600580.
44 Y. Nosaka and A. Y. Nosaka, *J. Phys. Chem. Lett.*, 2016, **7**, 431.
45 L. Chen, J. R. Wang, L. Q. Xie, C. Zhan, Z. Qiu, J. Z. Zhou, J. W. Yan, B. W. Mao and Z. Q. Tian, *Electrochem. Commun.*, 2016, **68**, 40.
46 F. Di Giacomo, V. Zardetto, G. Lucarelli, L. Cina, A. Di Carlo, M. Creatore and T. M. Brown, *Nano Energy*, 2016, **30**, 460.
47 H. Lu, W. Tian, B. K. Gu, Y. Y. Zhu and L. Li, *Small*, 2017, **13**, 052301.
48 Y. Z. Wu, X. D. Yang, H. Chen, K. Zhang, C. J. Qin, J. Liu, W. Q. Peng, A. Islam, E. B. Bi, F. Ye, M. S. Yin, P. Zhang and L. Y. Han, *Appl. Phys. Express*, 2014, **7**, 2130–2145.
49 H. Lu, Y. L. Ma, B. K. Gu, W. Tian and L. Li, *J. Mater. Chem. A*, 2015, **3**, 16445.
50 J. R. Lian, B. Lu, F. F. Niu, P. J. Zeng and X. W. Zhan, *Small Methods*, 2018, **2**, 916–921.
51 H. P. Zhou, Q. Chen, G. Li, S. Luo, T. B. Song, H. S. Duan, Z. R. Hong, J. B. You, Y. S. Liu and Y. Yang, *Science*, 2014, **345**, 542.
52 V. Zardetto, F. di Giacomo, H. Lifka, M. A. Verheijen, C. H. L. Weijtens, L. E. Black, S. Veenstra, W. M. M. Kessels, R. Andriessen and M. Creatore, *Adv. Mater. Interfaces*, 2018, **5**, 17999–18007.
53 J. P. C. Baena, L. Steier, W. Tress, M. Saliba, S. Neutzner, T. Matsui, F. Giordano, T. J. Jacobsson, A. R. S. Kandada, S. M. Zakeeruddin, A. Petrozza, A. Abate, M. K. Nazeeruddin, M. Gratzel and A. Hagfeldt, *Energy Environ. Sci.*, 2015, **8**, 2928.
54 J. P. Correa-Baena, W. Tress, K. Domanski, E. H. Anaraki, S. H. Turren-Cruz, B. Roose, P. P. Boix, M. Gratzel, M. Saliba, A. Abate and A. Hagfeldt, *Energy Environ. Sci.*, 2017, **10**, 1207.
55 Y. Lee, S. Lee, G. Seo, S. Paek, K. T. Cho, A. J. Huckaba, M. Calizzi, D. W. Choi, J. S. Park, D. Lee, H. J. Lee, A. M. Asiri and M. K. Nazeeruddin, *Adv. Sci.*, 2018, **5**, 1207–1212.
56 Y. Lee, S. Paek, K. T. Cho, E. Oveisi, P. Gao, S. Lee, J. S. Park, Y. Zhang, R. Humphry-Baker, A. M. Asiri and M. K. Nazeeruddin, *J. Mater. Chem. A*, 2017, **5**, 12729.
57 K. H. Jung, J. Y. Seo, S. Lee, H. Shin and N. G. Park, *J. Mater. Chem. A*, 2017, **5**, 24790.
58 Y. H. Kuang, V. Zardetto, R. van Gils, S. Karwal, D. Koushik, M. A. Verheijen, L. E. Black, C. Weijtens, S. Veenstra, R. Andriessen, W. M. M. Kessels and M. Creatore, *ACS Appl. Mater. Interfaces*, 2018, **10**, 30367.

59 C. L. Wang, L. Guan, D. W. Zhao, Y. Yu, C. R. Grice, Z. N. Song, R. A. Awni, J. Chen, J. B. Wang, X. Z. Zhao and Y. F. Yan, *ACS Energy Lett.*, 2017, **2**, 2118.
60 C. L. Wang, D. W. Zhao, C. R. Grice, W. Q. Liao, Y. Yu, A. Cimaroli, N. Shrestha, P. J. Roland, J. Chen, Z. H. Yu, P. Liu, N. Cheng, R. J. Ellingson, X. Z. Zhao and Y. F. Yan, *J. Mater. Chem. A*, 2016, **4**, 12080.
61 C. L. Wang, C. X. Xiao, Y. Yu, D. W. Zhao, R. A. Awni, C. R. Grice, K. Ghimire, I. Constantinou, W. Q. Liao, A. J. Cimaroli, P. Liu, J. Chen, N. J. Podraza, C. S. Jiang, M. M. Al-Jassim, X. Z. Zhao and Y. F. Yan, *Adv. Energy Mater.*, 2017, **7**, 14405–14408.
62 L. B. Xiong, Y. X. Guo, J. Wen, H. R. Liu, G. Yang, P. L. Qin and G. J. Fang, *Adv. Funct. Mater.*, 2018, **28**, 1802757.
63 J. Z. Chen and N. G. Park, *J. Phys. Chem. C*, 2018, **122**, 14039.
64 W. L. Tan, O. L. Hendricks, A. C. Meng, M. R. Braun, M. D. McGehee, C. E. D. Chidsey and P. C. McIntyre, *Adv. Mater. Interfaces*, 2018, **5**, 1800191.
65 S. Albrecht, M. Saliba, J. P. C. Baena, F. Lang, L. Kegelmann, M. Mews, L. Steier, A. Abate, J. Rappich, L. Korte, R. Schlatmann, M. K. Nazeeruddin, A. Hagfeldt, M. Gratzel and B. Rech, *Energy Environ. Sci.*, 2016, **9**, 81.
66 V. Zardetto, F. Di Giacomo, G. Lucarelli, W. M. M. Kessels, T. M. Brown and M. Creatore, *Sol. Energy*, 2017, **150**, 447.
67 B. J. Kim, D. H. Kim, Y. Y. Lee, H. W. Shin, G. S. Han, J. S. Hong, K. Mahmood, T. K. Ahn, Y. C. Joo, K. S. Hong, N. G. Park, S. Lee and H. S. Jung, *Energy Environ. Sci.*, 2015, **8**, 916.
68 J. H. Heo, M. H. Lee, H. J. Han, B. R. Patil, J. S. Yu and S. H. Im, *J. Mater. Chem. A*, 2016, **4**, 1572.
69 C. Zhang, D. W. Zhao, D. E. Gu, H. Kim, T. Ling, Y. K. R. Wu and L. J. Guo, *Adv. Mater.*, 2014, **26**, 5696.
70 T. Hu, T. Becker, N. Pourdavoud, J. Zhao, K. O. Brinkmann, R. Heiderhoff, T. Gahlmann, Z. Q. Huang, S. Olthof, K. Meerholz, D. Tobbens, B. C. Cheng, Y. W. Chen and T. Riedl, *Adv. Mater.*, 2017, **29**, 1606656.
71 S. Olthof and K. Meerholz, *Sci. Rep.*, 2017, **7**, 40267.
72 T. Leijtens, S. D. Stranks, G. E. Eperon, R. Lindblad, E. M. J. Johansson, I. J. McPherson, H. Rensmo, J. M. Ball, M. M. Lee and H. J. Snaith, *ACS Nano*, 2014, **8**, 7147.
73 P. Schulz, L. L. Whittaker-Brooks, B. A. MacLeod, D. C. Olson, Y. L. Loo and A. Kahn, *Adv. Mater. Interfaces*, 2015, **2**, 1400532.
74 Y. Yang, M. J. Yang, D. T. Moore, Y. Yan, E. M. Miller, K. Zhu and M. C. Beard, *Nat. Energy*, 2017, **2**, 16207.
75 L. Y. Wen, M. Zhou, C. L. Wang, Y. Mi and Y. Lei, *Adv. Energy Mater.*, 2016, **6**, 1600468.
76 A. K. Chandiran, A. Yella, M. T. Mayer, P. Gao, M. K. Nazeeruddin and M. Gratzel, *Adv. Mater.*, 2014, **26**, 4309.
77 A. K. Chandiran, M. Abdi-Jalebi, A. Yella, M. I. Dar, C. Y. Yi, S. A. Shivashankar, M. K. Nazeeruddin and M. Gratzel, *Nano Lett.*, 2014, **14**, 1190.
78 J. B. Zhang, A. Hultqvist, T. Zhang, L. C. Jiang, C. Q. Ruan, L. Yang, Y. B. Cheng, M. Edoff and E. M. J. Johansson, *ChemSusChem*, 2017, **10**, 3810.
79 S. S. Mali, C. S. Shim, H. K. Park, J. Heo, P. S. Patil and C. K. Hong, *Chem. Mater.*, 2015, **27**, 1541.
80 H. N. Si, Q. L. Liao, Z. Zhang, Y. Li, X. H. Yang, G. J. Zhang, Z. Kang and Y. Zhang, *Nano Energy*, 2016, **22**, 223.
81 S. Li, P. Zhang, Y. Wang, H. Sarvari, D. Liu, J. Wu, Y. Yang, Z. Wang and Z. D. Chen, *Nano Res.*, 2016, **10**, 1092.
82 X. Z. Yu, H. M. Yan and Q. Peng, *ACS Appl. Mater. Interfaces*, 2018, **10**, 28948.
83 X. Dong, X. Fang, M. H. Lv, B. C. Lin, S. Zhang, J. N. Ding and N. Y. Yuan, *J. Mater. Chem. A*, 2015, **3**, 5360.
84 I. S. Kim and A. B. F. Martinson, *J. Mater. Chem. A*, 2015, **3**, 20092.
85 D. Koushik, W. J. H. Verhees, Y. H. Kuang, S. Veenstra, D. Zhang, M. A. Verheijen, M. Creatore and R. E. I. Schropp, *Energy Environ. Sci.*, 2017, **10**, 91.
86 X. W. Hu, X. F. Jiang, X. B. Xing, L. Nian, X. Y. Liu, R. Huang, K. Wang, H. L. Yip and G. F. Zhou, *Sol. RRL*, 2018, **2**, 1800083.
87 J. M. Frost, K. T. Butler and A. Walsh, *APL Mater.*, 2014, **2**, 5122–5130.
88 M. I. Asghar, J. Zhang, H. Wang and P. D. Lund, *Renewable Sustainable Energy Rev.*, 2017, **77**, 131.
89 J. L. Yang, B. D. Siempelkamp, D. Y. Liu and T. L. Kelly, *ACS Nano*, 2015, **9**, 1955.
90 Y. Bai, Q. F. Dong, Y. C. Shao, Y. H. Deng, Q. Wang, L. Shen, D. Wang, W. Wei and J. S. Huang, *Nat. Commun.*, 2016, **7**, 12806.
91 C. Y. Chang, K. T. Lee, W. K. Huang, H. Y. Siao and Y. C. Chang, *Chem. Mater.*, 2015, **27**, 5122.
92 A. E. Shalan, S. Narra, T. Oshikiri, K. Ueno, X. Shi, H. P. Wu, M. M. Elshanawany, E. W. G. Diau and H. Misawa, *Sustainable Energy Fuels*, 2017, **1**, 1533.
93 I. S. Kim, D. H. Cao, D. B. Buchholz, J. D. Emery, O. K. Farha, J. T. Hupp, M. G. Kanatzidis and A. B. F. Martinson, *Nano Lett.*, 2016, **16**, 7786.
94 K. O. Brinkmann, J. Zhao, N. Pourdavoud, T. Becker, T. Hu, S. Olthof, K. Meerholz, L. Hoffmann, T. Gahlmann, R. Heiderhoff, M. F. Oszajca, N. A. Luechinger, D. Rogalla, Y. Chen, B. Cheng and T. Riedl, *Nat. Commun.*, 2017, **8**, 13938.
95 J. Zhao, K. O. Brinkmann, T. Hu, N. Pourdavoud, T. Becker, T. Gahlmann, R. Heiderhoff, A. Polywka, P. Gorrn, Y. Chen, B. Cheng and T. Riedl, *Adv. Energy Mater.*, 2017, **7**, 1602599.
96 L. Hoffmann, K. O. Brinkmann, J. Malerczyk, D. Rogalla, T. Becker, D. Theirich, I. Shutsko, P. Gorrn and T. Riedl, *ACS Appl. Mater. Interfaces*, 2018, **10**, 6006.
97 S. Seo, S. Jeong, C. Bae, N. G. Park and H. Shin, *Adv. Mater.*, 2018, **30**, 1801010.
98 A. Hultqvist, K. Aitola, K. Sveinbjornsson, Z. Saki, F. Larsson, T. Torndahl, E. Johansson, G. Boschloo and M. Edoff, *ACS Appl. Mater. Interfaces*, 2017, **9**, 29707.
99 A. F. Palmstrom, J. A. Raiford, R. Prasanna, K. A. Bush, M. Sponseller, R. Cheacharoen, M. C. Minichetti, D. S. Bergsman, T. Leijtens, H. P. Wang, V. Bulovic, M. D. McGehee and S. F. Bent, *Adv. Energy Mater.*, 2018, **8**, 1800591.
100 K. Domanski, J. P. Correa-Baena, N. Mine, M. K. Nazeeruddin, A. Abate, M. Saliba, W. Tress, A. Hagfeldt and M. Gratzel, *ACS Nano*, 2016, **10**, 6306.
101 A. Guerrero, J. B. You, C. Aranda, Y. S. Kang, G. Garcia-Belrnonte, H. P. Zhou, J. Bisquert and Y. Yang, *ACS Nano*, 2016, **10**, 218.
102 K. A. Bush, A. F. Palmstrom, Z. S. J. Yu, M. Boccard, R. Cheacharoen, J. P. Mailoa, D. P. McMeekin, R. L. Z. Hoye, C. D. Bailie, T. Leijtens, I. M. Peters, M. C. Minichetti, N. Rolston, R. Prasanna, S. Sofia, D. Harwood, W. Ma, F. Moghadam, H. J. Snaith, T. Buonassisi, Z. C. Holman, S. F. Bent and M. D. McGehee, *Nat. Energy*, 2017, **2**, 861–865.
103 G. E. Eperon, T. Leijtens, K. A. Bush, R. Prasanna, T. Green, J. T. W. Wang, D. P. McMeekin, G. Volonakis, R. L. Milot, R. May, A. Palmstrom, D. J. Slotcavage, R. A. Belisle, J. B. Patel, E. S. Parrott, R. J. Sutton, W. Ma, F. Moghadam, B. Conings, A. Babayigit, H. G. Boyen, S. Bent, F. Giustino, L. M. Herz, M. B. Johnston, M. D. McGehee and H. J. Snaith, *Science*, 2016, **354**, 861.
104 D. Yu, Y. Q. Yang, Z. Chen, Y. Tao and Y. F. Liu, *Opt. Commun.*, 2016, **362**, 43.
105 Q. Dong, F. Z. Liu, M. K. Wong, H. W. Tam, A. B. Djurisic, A. N. Ng, C. Surya, W. K. Chan and A. M. C. Ng, *ChemSusChem*, 2016, **9**, 2597.
106 T. J. Wilderspin, F. De Rossi and T. M. Watson, *Sol. Energy*, 2016, **139**, 426.
107 Y. I. Lee, N. J. Jeon, B. J. Kim, H. Shim, T. Y. Yang, S. I. Seok, J. Seo and S. G. Im, *Adv. Energy Mater.*, 2018, **8**, 1701928.
108 F. J. Ramos, T. Maindron, S. Bechu, A. Rebai, M. Fregnaux, M. Bouttemy, J. Rousset, P. Schulz and N. Schneider, *Sustainable Energy Fuels*, 2018, **2**, 2468.
109 Y. F. Lv, P. H. Xu, G. Q. Ren, F. Chen, H. R. Nan, R. Q. Liu, D. Wang, X. Tan, X. Y. Liu, H. Zhang and Z. K. Chen, *ACS Appl. Mater. Interfaces*, 2018, **10**, 23928.
110 J. Meyer, P. Görrn, F. Bertram, S. Hamwi, T. Winkler, H.-H. Johannes, T. Weimann, P. Hinze, T. Riedl and W. Kowalsky, *Adv. Mater.*, 2009, **21**, 1845.

 